Z_3 metastable states in PNJL model

Minati Biswal,[1,*] Sanatan Digal,[2,†] and P. S. Saumia[2,3,‡]
[1]*Institute of Physics, Bhubaneswar, 751005, India*
[2]*The Institute of Mathematical Sciences, Chennai, 600113, India*
[3]*Bogoliubov Laboratory of Theoretical Physics, JINR, 141980 Dubna, Russia*

(Received 24 July 2019; accepted 4 October 2020; published 26 October 2020)

We study the Z_3 metastable states in the Polyakov loop Nambu-Jona-Lasinio model. These states exist for temperatures above $T_m \sim 194$ MeV and can decay via bubble nucleation. We numerically solve the bounce equation to compute the nucleation rate. We speculate that, in the context of heavy-ion collisions, the likely scenario for the decay of the metastable states is via spinodal decomposition.

DOI: 10.1103/PhysRevD.102.074020

I. INTRODUCTION

In pure SU(N) gauge theories, energy density increases sharply across the critical temperature (T_c). It is believed that this is due to deconfinement of the constituents (gluons) of low energy excitations of the theory. This transition from confined to deconfined state of gluons, known as confinement-deconfinement (CD) transition, has been extensively studied in the literature [1–5]. The CD phase transition is found to be second order for $N = 2$ [6–11] and first order for $N \geq 3$ [12,13]. The Polyakov loop, which transforms as a Z_N spin, plays the role of an order parameter. It is real valued for $N = 2$ and complex for $N > 2$. Above the critical temperature, in a deconfined phase, it acquires a nonzero expectation value, spontaneously breaking the Z_N symmetry. This leads to N degenerate vacua. This nontrivial nature of the deconfined state allows for the existence of topological defects such as domain walls for $N = 2$ and domain walls connected by strings for $N > 2$ [14–16].

In a realistic theory such as quantum chromo dynamics (QCD), there are fermions (quarks) in the fundamental representation. The presence of these fermions leads to explicit breaking of the Z_N symmetry. The strength of the explicit symmetry breaking depends on the quark masses as well as the number of quark flavors [17–21]. It affects the nature of the CD transition [17,19] as well as the transition temperature. For large explicit symmetry breaking, the CD transition turns into a crossover while the transition temperature tends to decrease. Furthermore, there are no N degenerate vacua in the deconfined phase. Out of the previous N vacua, all but one becomes the ground state. With explicit symmetry breaking, the topological defects can still exist but far above T_c, and most of them are time dependent (nonstatic) [22].

The explicit breaking of the Z_N symmetry due to matter fields has been studied by calculating the partition function, or the effective potential of the Polyakov loop, when the gauge and matter field fluctuations are small [23–26]. These perturbative calculations are reliable for high temperatures ($T \gg T_c$), when the gauge coupling is expected to be small. Calculations which include fluctuations up to second order (one loop) show the presence of metastable states [20,23,25,27]. These states have been studied extensively in the context of cosmology. In the early Universe, they are found to be long lived and can leave observable imprints, while decaying nucleation of bubbles of true vacuum, as in a first order transition [27,28]. However, the number of effective quark flavors is larger than 3, in which case, the free energies of the metastable states, at one loop, are positive and hence lead to negative pressure and entropy [20]. This problem does not arise in QCD near the critical temperature as the number of flavors is effectively $\lesssim 3$.

The study of Z_3 metastable states for small temperatures, in particular near T_c, is important as they may affect the evolution of quark gluon plasma (QGP) in heavy-ion collision experiments. Near T_c perturbative calculations are expected to break down due to large gauge coupling constants and fluctuations. There are very few studies of Z_N symmetry using nonperturbative lattice QCD simulations. Lattice QCD results for 2 flavors show that out of the previous three degenerate vacua only one remains stable, while the other two become metastable states [21]. The two meta-stable states are degenerate, related via Z_2 symmetry. Furthermore, the metastability depends on the temperature

*minati.b@iopb.res.in
†digal@imsc.res.in
‡saumia@theor.jinr.ru

with the metastable states becoming unstable below $2T_c$ [21]. In general, nonperturbative lattice simulations are essential for a quantitative estimate of the explicit symmetry breaking; however, the mean field approaches provide a qualitative understanding. In a recent study of Z_3 symmetry in the Polyakov loop quark meson model [29], it is found that the metastable states exist above 310 MeV.

In heavy-ion collisions, the initial conditions are far from equilibrium. The system quickly thermalizes in less than a femtometer. In such a scenario, it is possible that the whole, or part, of the system can get trapped in one of the metastable states [28]. Also, if the system somehow thermalizes to a state of super hot hadron gas, which is a possibility at high baryon density, it will decay through bubble nucleation and some of the bubbles will have metastable cores.

In the present work, the Z_3 metastable states are studied in the Polyakov loop Nambu-Jona-Lasinio (PNJL) model at zero baryon chemical potential. In this model, they exist above $T_m \sim 194$ MeV. If such a state exists, then it can either become unstable (when temperature drops below T_m) or decay through nucleation of bubbles, which grow in real time converting the metastable state to stable state. To compute the nucleation rate, the Euler–Lagrange equation for the bubble/bounce solution [30–33] is numerically integrated. The action, as well as other properties of the bounce solution, is found to depend strongly on the temperature. This study finds that the likely scenario for the evolution/decay of a metastable state in heavy-ion collision is spinodal decomposition. This will lead to large oscillations of the Polyakov loop. We mention here that in heavy-ion collisions the baryon chemical potential is small but nonzero. At finite chemical potential, the thermodynamic potential has an imaginary part. There are several papers that discuss how to include the effect of nonzero μ [34,35]. With μ, the contribution of the fermions to the free energy will increase. Since the fermions break the Z_N symmetry, we expect that finite μ will lead to more explicit breaking. Following Roessner *et al.*, for small μ, we calculated the thermodynamic potential to the leading order, i.e., keeping only the real terms and found that T_m increases slightly with μ [29]. With increase in T_m there is lesser time available for the nucleation of bubbles, which enhances the likelihood of metastable states becoming unstable.

The paper is organized as follows. In Sec. II, Z_3 symmetry in pure $SU(3)$ gauge theory is discussed. We briefly go through the explicit breaking of Z_3 symmetry in the PNJL model and compute the thermodynamic properties of the metastable states in Sec. III. In Sec. IV, we present the calculation of the bounce solution. In Sec. V, we discuss the evolution of the metastable states in heavy-ion collisions and present our conclusions in Sec. VI.

II. Z_3 SYMMETRY IN PURE GAUGE THEORY

In path integral formulation, gauge fields, which are periodic in the temporal direction, only contribute to the partition function, i.e.,

$$A_\mu(\vec{x}, 0) = A_\mu(\vec{x}, \beta), \tag{1}$$

where $\beta = \frac{1}{T}$. This boundary condition allows for the gauge transformations $U(\vec{x}, \tau)$ to be periodic up to a factor $z \in Z_N$, such as

$$U(\vec{x}, 0) = zU(\vec{x}, \beta). \tag{2}$$

Though the partition function is invariant under the above gauge transformation, the Polyakov loop transforms as a Z_N spin. The Polyakov loop is defined as

$$L(\vec{x}) = \frac{1}{3}\mathrm{Tr}\left(\mathcal{P}\exp\left[ig\int_0^\beta d\tau A_0(\vec{x}, \tau)\right]\right). \tag{3}$$

Here $\mathcal{P}$ denotes path order, g is the gauge coupling, and $A_0 = A_0^a \frac{\tau^a}{2}$ is the temporal gauge field. Here τ_a are the Pauli matrices with a denoting the color indices. Under a Z_3 gauge transformation, Eq. (2), the Polyakov loop, transforms as $L(\vec{x}) \to zL(\vec{x})$. The thermal, as well as the volume average of the Polyakov loop $L(\vec{x})$,

$$L(T) = \left\langle \frac{1}{V}\int L(\vec{x})d^3x \right\rangle, \tag{4}$$

is related to the free energy $F_{\bar{Q}Q}(r)$ of a static (infinitely heavy) quark-antiquark pair at infinite separation [36]. Note

$$|L(T)|^2 = \exp\left[-\beta F_{\bar{Q}Q}(r = \infty)\right]. \tag{5}$$

In the following, we briefly describe the Z_3 symmetry in the effective potential for the Polyakov loop, which describes the CD transition in pure $SU(3)$ gauge theory [37]. We consider the following Landau–Ginsburg effective potential for a complex field Φ [37–39]:

$$U(\bar{\Phi}, \Phi, T) = b_4 T^4\left[-\frac{b_2(T)}{4}(|\Phi|^2 + |\bar{\Phi}|^2) - \frac{b_3}{6}(\Phi^3 + \bar{\Phi}^3) + \frac{1}{16}(|\Phi|^2 + |\bar{\Phi}|^2)^2\right]. \tag{6}$$

Different forms of the effective potential, in terms of the field Φ, have been proposed [38,40–44]. Across the critical temperature T_0, the Polyakov loop expectation value jumps discontinuously. The Z_3 symmetry and the first-order nature of the CD transition require a cubic term in the effective potential. The factor T^4 takes care of the dimension of the effective potential [37]. In the mean-field approximation, the minimum (minima) Φ_{th} of the effective

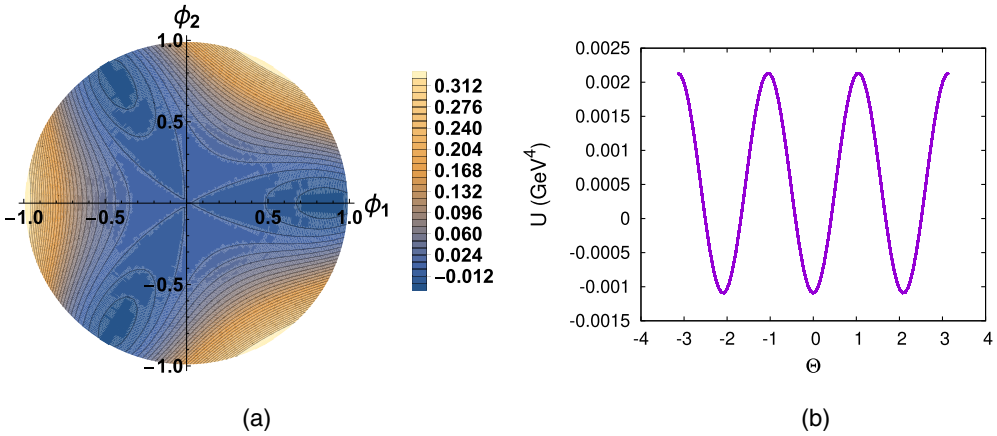

FIG. 1. (a) Contour plot for the Polyakov loop effective potential on the Φ_1—Φ_2 plane at $1.3T_0$. (b) Thermodynamic potential versus θ at $1.3T_0$.

potential gives the thermal average of the Polyakov loop $L(T)$. Note that $\Phi_{\rm th} = L(T)$. In this approximation, the pressure P is given by

$$\mathrm{P} = -U(\bar{\Phi}_{\rm th}, \Phi_{\rm th}, T). \tag{7}$$

The above effective potential with the following form of $b_2(T)$,

$$b_2(T) = (1 - 1.11T_0/T)(1 + 0.265T_0/T)^2 \times (1 + 0.3T_0/T)^3 - 0.487, \tag{8}$$

and the coefficients $b_3 = 2.0$ and $b_4 = 0.6016$, reproduces the pressure of the pure gauge theory computed from nonperturbative lattice method(s). Following [38], for QCD, b_4 is rescaled as $b_4 = 0.6061 \times 47.5/16$. Here, the coefficients are chosen such that the expectation value of the order parameter Φ approaches unity for $T \to \infty$. Hence, the fields and the coefficients in the above potential are rescaled as $\Phi \to \Phi/x$, $b_2(T) \to b_2(T)/x^2$, $b_3 \to b_3/x$, and $b_4 \to b_4/x^4$, where $x = b_3/2 + \frac{1}{2}\sqrt{b_3^2 + 4b_2(T=\infty)}$ for temperature $T \to \infty$. Note that we have used a polynomial form of the Polyakov loop potential, which is different from the more commonly used form as in [40]. The T_m for the latter case is higher than the initial temperature of QGP in heavy-ion collisions, which is not in agreement with lattice study [21]. Also, it is not clear that these models will be valid at such high temperatures.

For $T > T_0$, there are three degenerate minima in the effective potential, which can be seen in Fig. 1(a), the contour plot of the effective potential in the complex $\Phi = (\Phi_1, \Phi_2)$ plane at $T = 1.3T_0$. We also plot the variation of the potential along a circle going through the three minima, i.e., $\Phi = |\Phi_{\rm th}|e^{i\theta}$ in Fig. 1(b). The three degenerate vacua are situated at $\theta = 0$, $\frac{2\pi}{3}$, and $\frac{4\pi}{3}$, related by Z_3 rotation.

When dynamical quarks are included, the Z_3 symmetry is broken. While the pure gauge part of the action is Z_3 symmetric, the quark part of the action is not invariant under the Z_3 gauge transformations. This is because the gauge transformed quark fields are no longer antiperiodic along the temporal direction. The nontrivial Z_3 gauge transformations can act only on the gauge fields. The situation is similar to the presence of an external (explicit breaking) field in spin systems. For example, in the presence of an external field the Ising model Hamiltonian has both Z_2 symmetric and broken terms. As the magnetization still describes the Ising transition, the field Φ too describes the CD transition [45]. In the following section, we discuss the PNJL model, which provides a prescription to include the effect of quarks on the Z_3 symmetry and the Polyakov loop effective potential.

III. METASTABLE STATES IN PNJL MODEL

The PNJL model is an extension of the Nambu-Jona-Lasinio (NJL) model. The NJL model is a phenomenological model formulated on the basis of the chiral symmetry of QCD and describes the dynamics of low energy excitations, as well as the chiral transition [46–53]. Since there are no gauge fields in this model, it cannot describe the CD transition. The PNJL model attempts to include the gauge fields by adding the effective potential $U(\bar{\Phi}, \Phi, T)$ to the NJL Lagrangian [40,42,54–57]. Furthermore, in the fermion part of the NJL model, the covariant derivative substitutes the standard one. The PNJL Lagrangian is given by

$$\mathcal{L}_{\rm PNJL} = \sum_f (\bar{\Psi}_f(i\gamma_\nu D^\nu - m_f)\Psi_f + G_s[(\bar{\Psi}_f\tau_a\Psi_f)^2 + (\bar{\Psi}_f i\gamma_5\tau_a\Psi_f)^2]) + U(\bar{\Phi}, \Phi, T). \tag{9}$$

Here, D_ν is the covariant derivative, $D_\nu = \partial_\nu - i(gA_\nu + \delta_0^\nu\mu_f)$, $A_\nu = A_\nu^a\frac{\tau^a}{2}$. Here, subscript f refers to the u, d quark flavors. This term takes into account the interaction between the

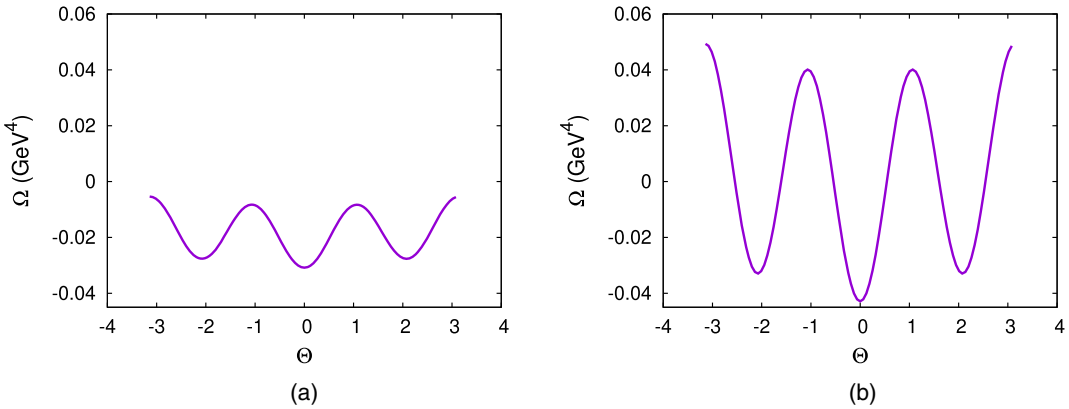

FIG. 2. Thermodynamic potential versus theta (a) at temperature 199.5 MeV and (b) at temperature 247 MeV. Note that σ value at each point is the one which minimizes Ω at the given value of θ.

gauge and quark fields. Note that m_f and μ_f are quark mass and chemical potential of quark flavor f, respectively. Note that G_s is the four quark contact interaction strength. The thermodynamic potential in the mean-field approximation for the above theory with two quark (u, d) flavors is given by [40,44]

$$\begin{aligned}\Omega = &-\sum_{f=u,d}\int_0^\infty \frac{d^3p}{(2\pi)^3}\,(2T\ln[1+3\Phi e^{-\beta(E_f-\mu_f)}+3\bar{\Phi}e^{-2\beta(E_f-\mu_f)}+e^{-3\beta(E_f-\mu_f)}]\\ &+2T\ln[1+3\bar{\Phi}e^{-\beta(E_f+\mu_f)}+3\Phi e^{-2\beta(E_f+\mu_f)}+e^{-3\beta(E_f+\mu_f)}])\\ &-6\sum_{f=u,d}\int\frac{d^3p}{(2\pi)^3}E_f\theta(\Lambda-|\vec{p}|)+\sum_{f=u,d}G_s\sigma_f^2+U(\bar{\Phi},\Phi,T).\end{aligned} \tag{10}$$

Here, $\sigma_f=\langle\bar{\Psi}\Psi\rangle_f$ is the quark condensate. Note that μ_u and μ_d are u and d quark chemical potentials, respectively. For the present calculations, chemical potentials are set to $\mu_u=\mu_d=0$. The masses of u and d quarks are taken to be degenerate, i.e., $m_u=m_d=m_0$. $E_{u,d}=\sqrt{p^2+\Sigma_{u,d}^2}$ are the single particle energies with $\Sigma_{u,d}=m_0-G_s\sigma_{u,d}-G_s\sigma_{d,u}$, where $G_s=10.08\ \mathrm{GeV}^{-2}$ and $m_0=5$ MeV. For $T_0=190$ MeV in the effective potential U, the thermodynamic potential given by Eq. (10) results in qualitatively similar thermodynamic behavior as that in [40,44].

For the temperature dependence of the quark condensates and expectation value of the Polyakov loop, we minimize the thermodynamic potential $\Omega(\sigma,m,T_0,T)$ by numerically solving the following set of equations:

$$\frac{\partial\Omega}{\partial\Phi_1}=0,\qquad \frac{\partial\Omega}{\partial\Phi_2}=0,\qquad \frac{\partial\Omega}{\partial\sigma}=0. \tag{11}$$

Note that Φ_1 and Φ_2 are real and imaginary parts of Φ. The numerical program requires initial trial values of Φ and σ. It evolves the trial values such that the thermodynamic potential decreases. The process stops once a minimum is reached within a certain numerical accuracy. This method cannot find all the minima at once. For each minima, the numerical procedure is repeated by suitable choices of initial conditions.

One can show that in the ground state Φ is real valued, i.e., $\Phi_2=0$ ($\theta=0$). Hence, for the ground state, we solve the above equations with initial values of $|\Phi|>0$ and $\theta=0$. We took the zero temperature value of σ as its initial value. For the metastable states, the Z_3 rotated values of the ground state Φ as the initial value works well. Since the Z_3 symmetry is explicitly broken, Z_3 rotated Φ does not solve the equations. However, the metastable states are found to be close to Z_3 rotations of the stable state. The value of σ in the metastable state is found to differ from the value in the stable state.

With the above numerical procedure, in the temperature range of $T_c(170)$ MeV—$T_m(194)$ MeV, only one solution is found with $\Phi_1>0$ and $\Phi_2=0$. Note that Z_3 rotated values of this solution as the initial condition does not result in any new solution. As the temperature is increased for $T>194$ MeV, two local minima appear around $\theta=\frac{2\pi}{3}$ and $\theta=-\frac{2\pi}{3}$. The thermodynamic potentials for these two states are found to be same but higher than that for the ground state, for which $\theta=0$. The values of Φ for the metastable and stable states are no more related by Z_3 rotation.

In Fig. 2, the thermodynamic potential versus θ has been plotted by fixing $|\Phi|$ in the stable state ($|\Phi|=0.79763$ for $T=199.5$ MeV and $|\Phi|=0.92962$ for 247 MeV) and minimizing thermodynamic potential with respect to σ. In Fig. 2(a) the temperature is close to T_m when the effective

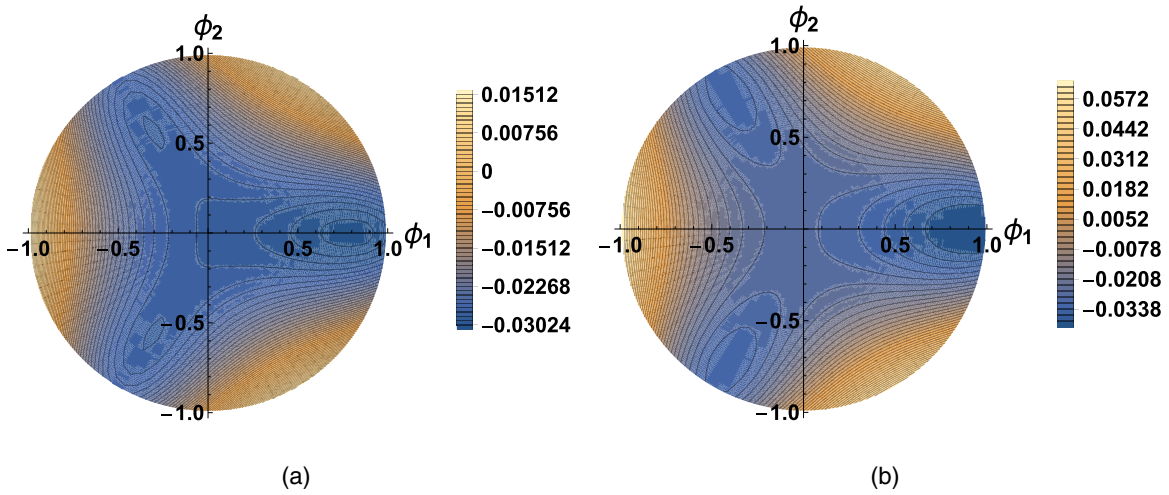

FIG. 3. Contour plot of the thermodynamic potential on the Φ_1—Φ_2 plane. (a) at temperature 199.5 MeV and (b) at temperature 247 MeV. Note that the σ value at each point is the one which minimizes Ω at the given Φ_1, Φ_2.

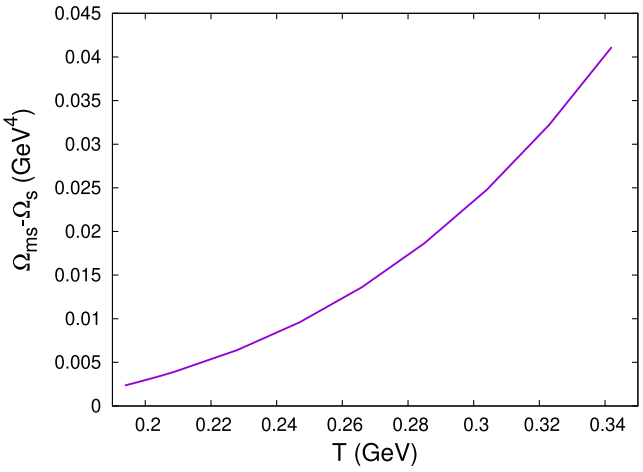

FIG. 4. The thermodynamic potential difference between metastable and stable states vs T.

potential develops two saddle points. Comparing Fig. 2(a) and Fig. 2(b) one can clearly see signs that the barrier between metastable and stable states increases with temperature. In Fig. 3, the contour plots of the thermodynamic potential in the $\Phi_1 - \Phi_2$ plane are shown. At each point Φ_1, Φ_2 in the contour plot, we have fixed σ at the value which minimises the thermodynamic potential. For temperatures above T_m, there are two metastable states and one stable state. We denote the metastable state for which $\Phi_2 < 0$ by M1 and the other by M2. The stable state is denoted by SS. Subscripts s and ms on variables denote their values in the stable state and the metastable states, respectively.

Figure 4 shows the difference in the thermodynamic potential of the metastable to the stable state ($\Omega_{ms} - \Omega_s$) vs T. This difference increases with temperature, which suggests enhancement in the explicit breaking for larger temperatures. In Fig. 5 we show the Polyakov loop in the M1, M2, and SS states for small values of μ. We find that with increase in μ the absolute value of the Polyakov loop

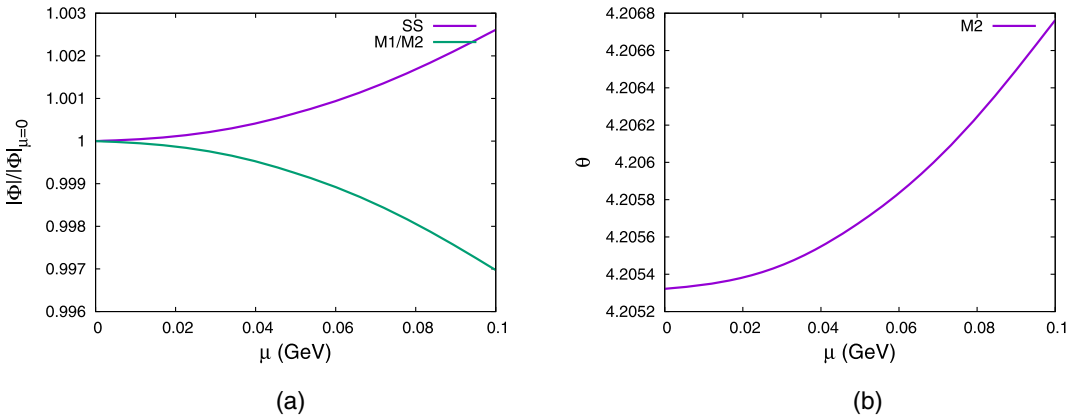

FIG. 5. Note μ dependence of the absolute value of Polyakov loop in the stable and metastable states normalized to the corresponding values at $\mu = 0$ (a) and the phase of the metastable state M2 (b).

decreases in the metastable states while it increases in the stable state. Note that the μ contribution effectively tilts the thermodynamic potential towards the stable state. We find that the phase of the M2 state shifts toward a higher value. The phase of M1 decreases as it is the complex conjugate of M2. We also find that the barrier height between (M1, M2) and SS decreases, while $T_m(\mu)$ increases slightly.

IV. BOUNCE SOLUTION FOR THE DECAY OF METASTABLE STATES

In the PNJL model with 2 quark flavors, metastable states exist above $T_m \sim 194$ MeV. Even though the value of T_m in this model is too small compared to the lattice result [21], we believe that it will give qualitative results for the effect of metastable states in heavy-ion collisions. We mention here that with other Polyakov loop potentials, higher T_m can be achieved by tuning the integration cut off in Eq. (10) though the results do not qualitatively differ from the present case.

As mentioned before, if a system is in the metastable state, then it will eventually decay to the stable state. A metastable state can either become unstable if the temperature drops below T_m or decay via nucleation of bubbles like in a first-order phase transition. At finite temperature, there will be fluctuations in the form of bubbles with stable states in their core. The free energy of a bubble consists of two components, the volume component and the surface component. The volume component comes from the free energy difference between the stable and the metastable states. The surface component comes from the fact that the fields (Φ, σ) have to interpolate between stable values at the center to metastable values outside. For a critical bubble, these two components balance, and a small fluctuation can make it grow or collapse. Thus, the critical bubble and its nucleation rate play an important role in a first-order phase transition. For decay of the state M1(M2), the fields Φ and σ will have values corresponding to the SS inside the bubble. Both these fields vary smoothly across the bubble wall and approach the values corresponding to M1(M2). Given that the free energy does not depend on the sign of Φ_2, the bubbles interpolating M1 and SS will have the same action as the other interpolating M2 and SS. The critical bubble is obtained from the bounce solution, which is a saddle point of the Euclidean action. We must mention here that the bubble nucleation picture here is not related to any phase transition but to the fact that the theory allows existence of metastable states above a certain temperature, and they can tunnel into the stable state.

The decay rate of the false vacuum (metastable state) can be calculated in the semiclassical approximation where the dominant contribution comes from the configurations with the least action [30,31], i.e., bounce solutions. It is shown that such configurations at zero temperatures have $O(4)$ symmetry, reducing the problem to 1 degree of freedom along the radial direction given by $r^2 = |\mathbf{x}|^2 + \tau^2$ in the Euclidean space. It has been shown that the problem is equivalent to calculating the classical evolution of a particle in the Euclidean space in the presence of the inverted potential $-V(\phi)$, where the particle rolls down from the stable vacuum and bounces up to the metastable one. The decay rate then can be written as the summation of all such "bounces" [30]. At high temperatures, owing to the periodicity of the field theory in the "time" direction, the field configurations will have $O(3)$ symmetry on a time slice [32]. For a single scalar field theory with a metastable state, the bounce can then be calculated by solving the equation of motion

$$\frac{d^2\phi}{dr^2} + \frac{2}{r}\frac{d\phi}{dr} = \frac{\partial V}{\partial \phi}, \tag{12}$$

with the boundary conditions $\phi \to \phi^m$ as $r \to \infty$, where ϕ^m is the value of the field in the metastable state. For $r \sim 0$ the field is expected to be close to the stable state. If r were the time variable, then Eq. (12) would be the equation of motion of a particle in an inverted potential with a damping term. The required boundary conditions are equivalent to the trajectory of a particle starting from the maximum of the inverted potential (which corresponds to the stable state), rolling down, and climbing up to the local maximum, which corresponds to the metastable point. As the particle approaches the local maximum, its velocity approaches zero. The critical bubble nucleation probability rate per unit of volume at finite temperature is proportional to $\exp(-S/T)$, where S is the action of the bounce solution.

A. The bounce

The bounce Eq. (12) is nonlinear in ϕ, which makes it difficult to solve analytically. Only in the thin-wall approximation, when the stable and metastable are almost degenerate, can the bounce be calculated analytically. Such an approximation will not be valid in the present case as the difference in the thermodynamic potential between the stable and metastable states increases with T and dominates the barrier height. Hence, numerical integration is the only way to find the bounce/bubble profile. The numerical integration is straightforward when there is a symmetry, for example, in $U(1)$ theory where only the radial mode of the field appears in the bounce equation. The phase is taken to be uniform, for minimum action bubble profile.

In the PNJL model there is no such symmetry, the real and imaginary parts of Polyakov loop field and the sigma field are expected to have nontrivial profiles. Since evolving all the three fields simultaneously proved extremely difficult, we kept the sigma field constant throughout the trajectory, that is, σ is independent of r. Later we will consider sample profiles for σ to estimate the corrections to the action. We also calculate the lower bound of the action. In the present case, the thermodynamic potential

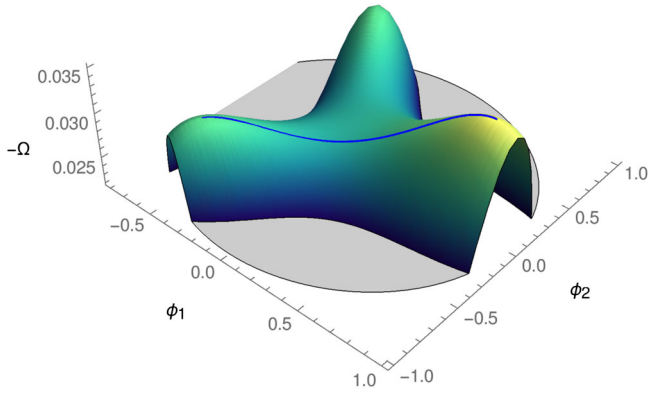

FIG. 6. Plot of the inverted potential in the Polyakov loop plane. The blue trajectory is the bounce solution at 228 MeV.

$\Omega(\Phi_1, \Phi_2, \sigma)$ replaces $V(\phi)$ in Eq. (12). The equations to be solved simultaneously are given by

$$\frac{d^2\Phi_1}{dr^2} + \frac{2}{r}\frac{d\Phi_1}{dr} = \frac{\partial\Omega}{\partial\Phi_1}$$
$$\frac{d^2\Phi_2}{dr^2} + \frac{2}{r}\frac{d\Phi_2}{dr} = \frac{\partial\Omega}{\partial\Phi_2}. \tag{13}$$

The boundary conditions are $\Phi_i \to \Phi_i^m$ as $r \to \infty$. Note that Φ_i^m, $i = 1, 2$ are the values of Φ_1, Φ_2 in the metastable state. For the numerical integration, r is discretized as $r \to r_n = n\delta$, where δ is the lattice spacing. Note that δ must be smaller compared to the length scale of typical variations of Φ. The integration starts from $r = r_0 \sim 0$. Two types of discretizations of Eq. (13) are considered. In the first approach, the values of Φ_1, Φ_2 at $r = r_0$ and $r = r_0 + \delta$ are used to generate the trajectory. In the second approach the two equations are rewritten as 4 first-order equations. In this case, the values of Φ_1, Φ_2, as well as their derivatives at r_0, determine the trajectory. It has been checked that both of these methods of integration give the same results. A few other approaches to calculating bounce solution for multiple field cases are discussed in [58–65].

In Fig. 6 we show the plot of the inverted potential in the Polyakov loop plane. There is a ridge which connects the stable and metastable states. The height of the ridge initially drops from the stable peak but eventually rises to the metastable peak. The bounce profile must start near the stable state and approach the metastable state. This can happen only for a unique choice of initial conditions, i.e., position (Φ_1, Φ_2) and velocity $(\frac{d\Phi_1}{dr}, \frac{d\Phi_2}{dr})$. For wrong choices, the trajectory will fall off to infinity either through the center along $\theta = \pi$ or by crossing the ridge to $\theta \sim -\pi/3$. Hence, the initial conditions must be tuned, which is achieved by a standard bisection method. The basic idea is that with the given initial conditions, position $(\Phi_1(r_0), \Phi_2(r_0))$ and velocity $(\frac{d\Phi_1}{dr}|_{r_0}, \frac{d\Phi_2}{dr}|_{r_0})$, if a trajectory undershoots (overshoots) the metastable point (peak), then we start with an initial choice (position) closer to (farther from) the "global" minimum (global peak). Furthermore, the bisection method is used to find the direction of initial velocity such that the undershoot trajectory makes a 180° turn or the overshoot trajectory passes through the metastable state peak. We have checked that the results do not change for smaller δ.

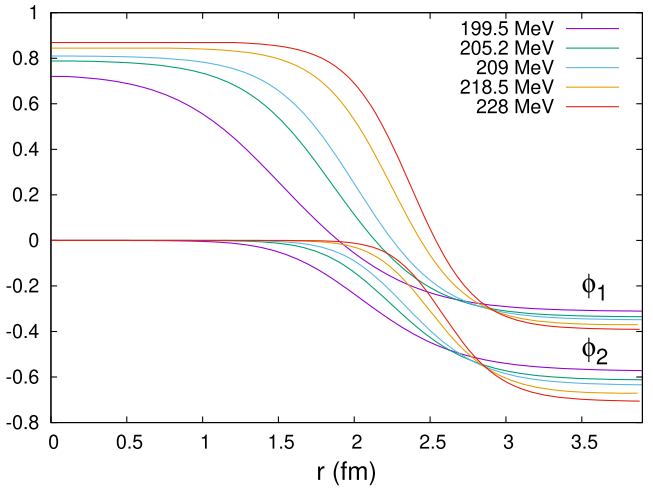

FIG. 7. Bubble profiles for Φ_1 and Φ_2 at different temperatures.

B. The bubble

The bubble profiles are computed for temperatures in the range $T = 1.05T_0 - 1.2T_0$, i.e., 199.5 MeV to 228 MeV. Figure 7 shows the temperature dependence of the bubble profiles. These bubble profiles represent the decay of M1 to SS. The values of Φ_1 and Φ_2 approach asymptotically to their corresponding metastable values. For temperatures just above T_m, the barrier between the stable and metastable states is small compared to $\Omega_s - \Omega_{ms}$. Starting with the initial values of the field close to Φ_i^s at $r_0 \sim 0$ will always lead to overshooting. Hence, the initial values of the fields (at the center of the bubble) must be farther away from the stable point. Since the field starts already on a higher slope for small r, damping dominates the profile giving a broad "wall" profile for the bounce. For higher temperatures, the initial point is closer to the stable point. The force term is small; so is acceleration. The field gets to spend more time near the stable state. Therefore, the core radius of the bubble increases as we go towards higher temperatures. The bubble wall is thinner because the particle/field spends larger time near the stable maximum and when it eventually starts rolling, the damping is small.

Figure 8 shows the radii of these bubbles as a function of temperature. We define the radius of the bubble as the radial distance from the center to the point where the field drops half way to the metastable value. Here, we notice that the radii for the two different fields are not the same. The radius

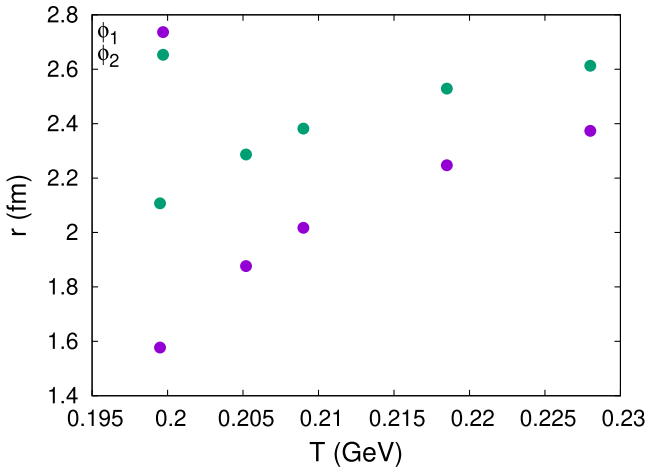

FIG. 8. Bubble radii vs temperature.

of the Φ_2 profile is slightly higher than that of Φ_1. This is because the curvature of the potential along Φ_1 and Φ_2, or in other words, their mass scales, are different.

Figure 9 (left) shows a plot of the θ profile of the bubble at $T = 218.5$ MeV. We also plot the magnitude of the Polyakov loop versus radius in Fig. 9 (right).

V. EVOLUTION OF METASTABLE STATE IN HEAVY-ION COLLISIONS

The decay rate of these metastable states depends on the bubble action, which is given by

$$S = \int 4\pi r^2 dr \left[\frac{1}{2}\alpha T^2 \left\{\left(\frac{d\Phi_1}{dr}\right)^2 + \left(\frac{d\Phi_2}{dr}\right)^2\right\} + \frac{1}{2}G_s^2\left(\frac{d\sigma}{dr}\right)^2 + \Omega(\Phi_1, \Phi_2, \sigma)\right]. \quad (14)$$

Here, α is a constant given by $2N/g^2$ [38], where N is the number of colors, and g is the gauge coupling constant. For $g/4\pi = 0.3$, $\alpha = 1.6$. Figure 10(a) shows the plot of the bubble action in units of temperature vs T. Let us recall here that σ was kept constant at the metastable value in the bubble. For an estimate of the change in the action, an

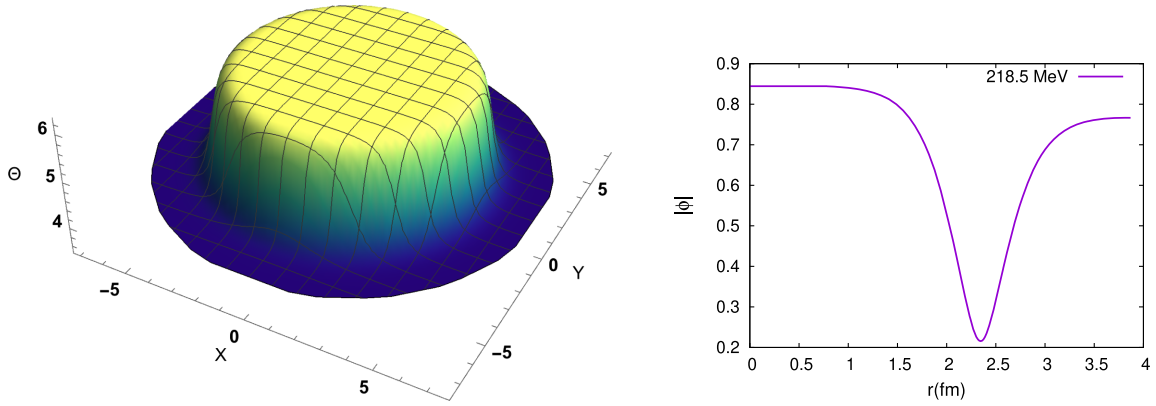

FIG. 9. Plot of θ field for the bubble (left) and modulus of Φ vs radius (right) at 218.5 MeV.

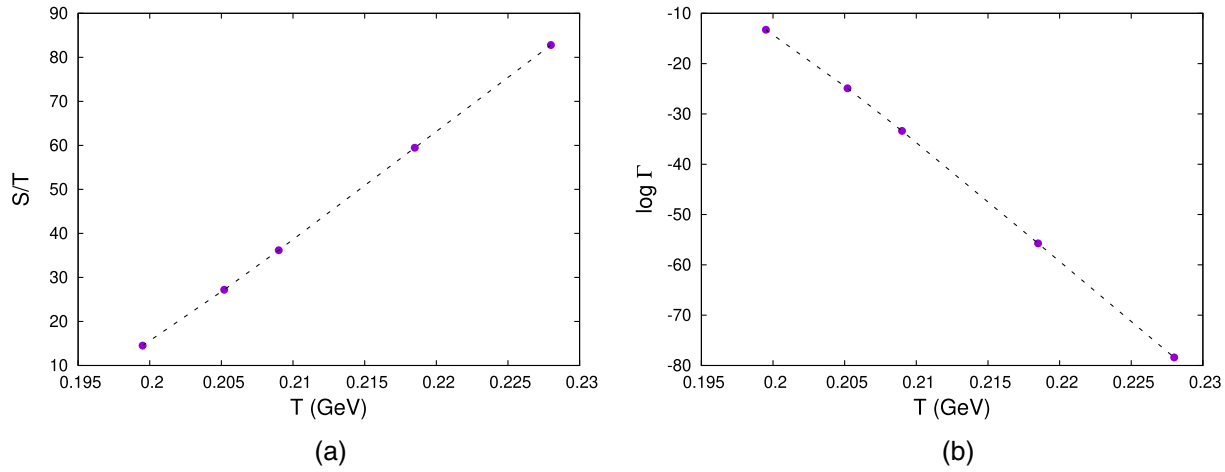

FIG. 10. (a) Bubble action in units of T and (b) Log of the bubble nucleation rate (per fm^3 per fm time) vs T.

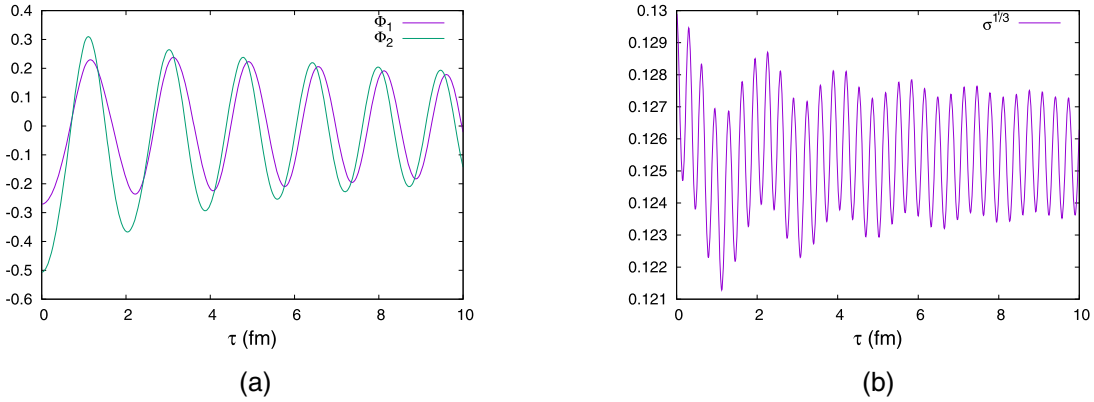

FIG. 11. Evolution of (a) Polyakov loop and (b) $\sigma^{1/3}$ after the temperature falls below T_m. Here, $\tau = 0$ corresponds to the time at which temperature is below T_m.

approximate σ profile is computed by minimizing Ω with respect to σ for a given Φ_1, Φ_2 profile. With the σ profile the bubble action decreases slightly. The decrement is below 10% for all the temperatures calculated. We also checked with σ profiles scaled like both Φ_1 and Φ_2 profiles, interpolating between $\sigma_s - \sigma_{ms}$. In the case where the σ profile was scaled like Φ_1, the action was minimum (less than 20% decrement).

The bubble nucleation probability per unit time per unit volume, or in other words, the decay rate of the metastable state is given by [32]

$$\Gamma = T^4 \left(\frac{S}{2\pi T}\right)^{3/2} \exp(-S/T). \tag{15}$$

One can see from Fig. 10(b) that this value is as small as 10^{-6}/ fm for the smallest temperature above T_m (199.5 MeV) and grows insignificantly for higher temperatures. Though it is difficult to solve for the bubble in the full case by including an equation corresponding to σ in Eq. (13), we can compute the lower bound of the full action. The corresponding nucleation rate will then be the upper bound. Note that Γ has a peak in S/T. However, for the range of S/T in our calculation, Γ is a monotonically decreasing function of S/T. To compute the upper bound on the nucleation rate, we fix the σ field at the SS value (σ_s). To see how $\sigma(r) = \sigma_s$ leads to this bound, we write the free energy (F_b) of a critical bubble of radius R_d as

$$F_b = -\frac{4\pi}{3}\rho R_d^3 + 4\pi\delta R_d^2, \qquad R_d = \frac{2\delta}{\rho}, \tag{16}$$

where ρ is the free energy difference between the stable and metastable state, and δ is the free energy cost (surface tension) as the fields vary smoothly between the two states. The position of the metastable state when the σ is fixed at σ_s deviates from the full case such that $|\Phi_s - \Phi_{ms}|$ decreases. This effectively leads to a decrease in δ. Also with $\sigma = \sigma_s$, the metastable states always have higher Ω_{ms} compared to the full case. This leads to an increase in ρ. Hence, the free energy for $\sigma = \sigma_s$ is lower compared to the full case. Note that the barrier height also plays a role in determining δ, which is the reason the bubble action grows with temperature. However, for a given temperature the barrier would slightly decrease as σ changes from σ_{ms} to σ_s.

We do a quick calculation of the decay rate for the case of heavy-ion collisions, assuming the thermalization time to be $\tau_i = 0.38$ fm and the initial temperature of the order of $T_i \sim 550$ MeV. We consider the QGP to be cylindrical (the midrapidity region) with radius 8 fm and length 3 fm. The number of bubbles nucleated within this volume when the system cools down to a temperature T is estimated as follows. The bubble action S as a function of temperature is obtained by fitting our data points. We used a longitudinally boost invariant $2+1D$ hydrodynamic simulation with Glauber optical initial conditions following [66], to fit the temperature evolution. The number of bubbles nucleated in volume V during the time τ when the temperature drops to T is given by

$$N(\tau) = V \int_{\tau_i}^{\tau} \Gamma(t) dt. \tag{17}$$

We find that $N(T_m) = N(\tau_m)$, where τ_m is the time at which temperature is T_m, is vanishingly small. Here, we have used the profile with sigma scaled as Φ_1. If any of the other profiles are used, then this number only decreases. The value of $N(\tau)$ rapidly decreases for higher temperatures. If we assume a larger equilibration time, that is, a smaller initial temperature, then the value of $N(\tau)$ decreases further. We have also computed the free energy of the bubble (action) and the nucleation rate by fixing $\sigma = \sigma_s$. We find that the bubble action is smaller by an average factor of $\sim$0.45 compared to the case when σ is fixed at σ_{ms}. In this calculation the nucleation rate increases by a factor of one hundred, though still remaining negligibly small. We have considered the effects of μ up to $\sim$100 MeV. For $\mu = 100$ MeV, T_m increases by $\sim$2 MeV. Since the barrier height decreases with μ, the bubble action

$S(T,\mu) < S(T,\mu=0)$. However, the system spends less time above $T_m(\mu)$, hence the results will not change qualitatively. Hence, we do not expect any bubble nucleation in heavy ion collisions. This leads to an interesting scenario known as the spinodal decomposition. When the metastable states become unstable below T_m, the field will roll down to the minimum resulting in large angular fluctuations. Figure 11 shows the evolution of the Polyakov loop and chiral condensate at the center of the quark gluon plasma after the temperature falls below T_m at zero chemical potential. Since the metastable states become unstable, the fields roll down and oscillate around the minimum. These oscillations will have interesting consequences in the dynamics of heavy-ion collisions including flow, jet energy loss [67], and also may possibly lead to coherent emission of particles. As discussed above, at a small finite chemical potential, $T_m(\mu)$ increases, and spinodal decomposition is expected to occur earlier.

VI. CONCLUSIONS

We have studied the Z_3 metastable states in the PNJL model. The metastable states exist at and above the temperature $T_m \sim 194$ MeV. For small values of μ, we found that T_m increases slightly, i.e., by ~ 2 MeV at $\mu = 100$ MeV. The barrier height between the metastable and stable states decreases. We have discussed the probability of the decay of these metastable states by calculating the stable bubble nucleation probability in the metastable regions using bounce solution. The bubble action measured in the units of temperature increases roughly linear in temperature. For small μ, relevant for heavy-ion collisions, the bubble action decreases slightly though the system spends lesser time above T_m. Our results suggest that the probability of these states decaying by tunneling into stable states is very small in the case of heavy-ion collisions. Ultimately the metastable state will become unstable, and the fields will start rolling towards the minimum. This will lead to large oscillations of the Polyakov loop field, which may have interesting consequences to the dynamics of flow, jet energy loss, and also may lead to coherent emission of particles.

ACKNOWLEDGMENTS

We thank A. P. Balachandran, Shreyansh S. Dave, Ajit Srivastava, Rajarshi Ray and Ranjita Mohapatra for important comments and suggestions.

[1] J. Kuti, J. Polonyi, and K. Szlachanyi, Phys. Lett. **98B**, 199 (1981).
[2] T. Celik, J. Engels, and H. Satz, Phys. Lett. **125B**, 411 (1983).
[3] L. Susskind, Phys. Rev. D **20**, 2610 (1979).
[4] J. Engels, F. Karsch, H. Satz, and I. Montvay, Phys. Lett. **101B**, 89 (1981).
[5] F. Karsch, Lect. Notes Phys. **583**, 209 (2002).
[6] P. H. Damgaard, Phys. Lett. B **194**, 107 (1987).
[7] J. Engels, J. Fingberg, K. Redlich, H. Satz, and M. Weber, Z. Phys. C **42**, 341 (1989).
[8] J. Christensen and P. H. Damgaard, Nucl. Phys. **B348**, 226 (1991).
[9] P. H. Damgaard and M. Hasenbusch, Phys. Lett. B **331**, 400 (1994).
[10] J. Engels, F. Karsch, and K. Redlich, Nucl. Phys. **B435**, 295 (1995).
[11] J. Engels and T. Scheideler, Nucl. Phys. **B539**, 557 (1999).
[12] G. Boyd, J. Engels, F. Karsch, E. Laermann, C. Legeland, M. Lutgemeier, and B. Petersson, Phys. Rev. Lett. **75**, 4169 (1995).
[13] G. Boyd, J. Engels, F. Karsch, E. Laermann, C. Legeland, M. Lutgemeier, and B. Petersson, Nucl. Phys. **B469**, 419 (1996).
[14] A. P. Balachandran and S. Digal, Int. J. Mod. Phys. A **17**, 1149 (2002).
[15] B. Layek, A. P. Mishra, and A. M. Srivastava, Phys. Rev. D **71**, 074015 (2005).
[16] U. S. Gupta, R. K. Mohapatra, A. M. Srivastava, and V. K. Tiwari, Phys. Rev. D **82**, 074020 (2010).
[17] F. Green and F. Karsch, Nucl. Phys. **B238**, 297 (1984).
[18] M. Oevers, F. Karsch, E. Laermann, and P. Schmidt, Nucl. Phys. B, Proc. Suppl. **63**, 394 (1998).
[19] F. Karsch, E. Laermann, A. Peikert, C. Schmidt, and S. Stickan, Nucl. Phys. B, Proc. Suppl. **94**, 411 (2001).
[20] V. M. Belyaev, I. I. Kogan, G. W. Semenoff, and N. Weiss, Phys. Lett. B **277**, 331 (1992).
[21] M. Deka, S. Digal, and A. P. Mishra, Phys. Rev. D **85**, 114505 (2012).
[22] U. S. Gupta, R. K. Mohapatra, A. M. Srivastava, and V. K. Tiwari, Phys. Rev. D **86**, 125016 (2012).
[23] D. J. Gross, R. D. Pisarski, and L. G. Yaffe, Rev. Mod. Phys. **53**, 43 (1981).
[24] N. Weiss, Phys. Rev. D **24**, 475 (1981).
[25] N. Weiss, Phys. Rev. D **25**, 2667 (1982).
[26] Y. Guo and Q. Du, J. High Energy Phys. 05 (2019) 042.
[27] V. Dixit and M. C. Ogilvie, Phys. Lett. B **269**, 353 (1991).
[28] J. Ignatius, K. Kajantie, and K. Rummukainen, Phys. Rev. Lett. **68**, 737 (1992).
[29] H. Mishra and R. K. Mohapatra, Phys. Rev. D **95**, 094014 (2017).
[30] S. R. Coleman, Phys. Rev. D **15**, 2929 (1977); **16**, 1248(E) (1977).
[31] C. G. Callan, Jr. and S. R. Coleman, Phys. Rev. D **16**, 1762 (1977).

[32] A. D. Linde, Nucl. Phys. **B216**, 421 (1983); **B223**, 544(E) (1983).
[33] M. Gleiser, E. W. Kolb, and R. Watkins, Nucl. Phys. **B364**, 411 (1991).
[34] A. Dumitru, R. D. Pisarski, and D. Zschiesche, Phys. Rev. D **72**, 065008 (2005).
[35] S. Roessner, T. Hell, C. Ratti, and W. Weise, Nucl. Phys. **A814**, 118 (2008).
[36] B. Svetitsky, Phys. Rep. **132**, 1 (1986).
[37] R. D. Pisarski, Phys. Rev. D **62**, 111501 (2000).
[38] A. Dumitru and R. D. Pisarski, Phys. Lett. B **504**, 282 (2001).
[39] A. Dumitru and R. D. Pisarski, Nucl. Phys. B, Proc. Suppl. **106**, 483 (2002).
[40] C. Ratti, M. A. Thaler, and W. Weise, Phys. Rev. D **73**, 014019 (2006).
[41] C. Ratti, S. Roessner, M. A. Thaler, and W. Weise, Eur. Phys. J. C **49**, 213 (2007).
[42] S. Roessner, C. Ratti, and W. Weise, Phys. Rev. D **75**, 034007 (2007).
[43] A. Bhattacharyya, P. Deb, A. Lahiri, and R. Ray, Phys. Rev. D **82**, 114028 (2010).
[44] S. K. Ghosh, T. K. Mukherjee, M. G. Mustafa, and R. Ray, Phys. Rev. D **77**, 094024 (2008).
[45] J. Engels, V. K. Mitrjushkin, and T. Neuhaus, Nucl. Phys. B, Proc. Suppl. **34**, 298 (1994).
[46] Y. Nambu and G. Jona-Lasinio, Phys. Rev. **122**, 345 (1961).
[47] Y. Nambu and G. Jona-Lasinio, Phys. Rev. **124**, 246 (1961).
[48] S. P. Klevansky, Rev. Mod. Phys. **64**, 649 (1992).
[49] U. Vogl and W. Weise, Prog. Part. Nucl. Phys. **27**, 195 (1991).
[50] O. Scavenius, A. Mocsy, I. N. Mishustin, and D. H. Rischke, Phys. Rev. C **64**, 045202 (2001).
[51] T. Hatsuda and T. Kunihiro, Phys. Rep. **247**, 221 (1994).
[52] M. Buballa, Phys. Rep. **407**, 205 (2005).
[53] F. Gastineau, R. Nebauer, and J. Aichelin, Phys. Rev. C **65**, 045204 (2002).
[54] S. Mukherjee, M. G. Mustafa, and R. Ray, Phys. Rev. D **75**, 094015 (2007).
[55] P. Costa, C. A. de Sousa, M. C. Ruivo, and H. Hansen, Europhys. Lett. **86**, 31001 (2009).
[56] S. K. Ghosh, T. K. Mukherjee, M. G. Mustafa, and R. Ray, Indian J. Phys. **85**, 87 (2011).
[57] P. Deb, A. Bhattacharyya, S. K. Ghosh, R. Ray, and A. Lahiri, Nucl. Phys. **A862-A863**, 267 (2011).
[58] T. Konstandin and S. J. Huber, J. Cosmol. Astropart. Phys. 06 (2006) 021.
[59] C. L. Wainwright, Comput. Phys. Commun. **183**, 2006 (2012).
[60] M. L. Piscopo, M. Spannowsky, and P. Waite, Phys. Rev. D **100**, 016002 (2019).
[61] A. Masoumi, K. D. Olum, and B. Shlaer, J. Cosmol. Astropart. Phys. 01 (2017) 051.
[62] P. Athron, C. Balzs, M. Bardsley, A. Fowlie, D. Harries, and G. White, Comput. Phys. Commun. **244**, 448 (2019).
[63] R. Sato, Phys. Rev. D **101**, 016012 (2020).
[64] S. Profumo, L. Ubaldi, and C. Wainwright, Phys. Rev. D **82**, 123514 (2010).
[65] S. Chigusa, T. Moroi, and Y. Shoji, Phys. Lett. B **800**, 135115 (2020).
[66] P. F. Kolb, J. Sollfrank, and U. W. Heinz, Phys. Rev. C **62**, 054909 (2000).
[67] S. Lin, R. D. Pisarski, and V. V. Skokov, Phys. Lett. B **730**, 236 (2014).